

The promising path of evolutionary optimization to avoid barren plateaus

Jakab Nádori,¹ Gregory Morse,² Zita Majnay-Takács,² Zoltán Zimborás,^{2,3,4}
Péter Rakyta,^{1,3*}

¹Department of Physics of Complex Systems, Eötvös Loránd University, Budapest, Hungary

²Department of Programming Languages and Compilers, Eötvös Loránd University,
Budapest, Hungary

³Wigner Research Center for Physics, P.O. Box 49, 1525 Budapest, Hungary

⁴Algorithmiq Ltd, Kanavakatu 3C 00160 Helsinki, Finland

*To whom correspondence should be addressed; E-mail: peter.rakyta@ttk.elte.hu.

Variational quantum algorithms are viewed as promising candidates for demonstrating quantum advantage on near-term devices. These approaches typically involve the training of parameterized quantum circuits through a classical optimization loop. However, they often encounter challenges attributed to the exponentially diminishing gradient components, known as the barren plateau (BP) problem. This work introduces a novel optimization method designed to alleviate the adverse effects of BPs during circuit training. Our approach to select the optimization search direction relies on the distant features of the cost-function landscape. This enables the optimization path to navigate around barren plateaus without the need for external control mechanisms. We have successfully applied our optimization strategy to quantum circuits comprising 16 qubits and 15000 entangling gates, demonstrating robust resistance against BPs. Additionally, we have extended our optimization strategy by incorpo-

rating an evolutionary selection framework, enhancing its ability to avoid local minima in the landscape. The modified algorithm has been successfully utilized in quantum gate synthesis applications, showcasing a significantly improved efficiency in generating highly compressed quantum circuits compared to traditional gradient-based optimization approaches.

Introduction

The Variational Quantum Eigensolver (VQE) originally formulated by Peruzzo et al. (1) and McClean et al. (2), has garnered considerable attention within the research community over the past two decades (3). VQE uses the variational principle to calculate the ground state energy of a Hamiltonian, a fundamental problem in quantum chemistry and condensed matter physics. Conventional computing methods face limitations in accuracy and efficiency, due to the exponentially growing complexity of the quantum state used to describe many-body systems. VQE, on the other hand, is expected to be efficient to model these complex wave-functions in polynomial time, making it one of the most promising near-term applications for quantum computing. In addition, variational quantum algorithms have demonstrated some degree of resilience to noise in the quantum hardware, making them a good candidate to deliver reasonable calculation results even on near-term quantum computers. Consequently, VQE stands as a prominent example of NISQ algorithms. In its most general form, it seeks to compute an upper bound for the ground-state energy of a Hamiltonian, typically provide the first step to determine the energetic properties of molecules and materials. The potential applications of VQE are therefore extensive, encompassing areas such as drug discovery (4, 5), material science (6), chemical engineering (7–9), quantum optimization (10, 11), and quantum machine learning (12, 13).

While the training process in variational quantum algorithms is proven to be NP-Hard (14), the literature highlights four primary areas of research aimed at bringing VQE closer to practical

real-world applications. These areas encompass: (i) The development of optimal measurement techniques to minimize the required number of circuit repetitions for VQE execution. (ii) The establishment of extensive parallelization methods across multiple quantum computers. (iii) The creation of strategies to address potential challenges associated with vanishing gradients during the optimization process for larger systems. (iv) The exploration of tailored error mitigation approaches specifically designed for the VQE algorithm. The solutions to these open research questions will show the pathways for VQEs to attain quantum advantage, particularly as quantum computing hardware scales up and noise levels hopefully diminish.

In this study, we address a common pitfall encountered in variational quantum algorithms during parameter optimization, known as the barren plateau (BP) problem, as described in prior research (15–17). The BP arises due to the phenomenon where the gradients of the cost function vanish exponentially as the number of qubits in the quantum model increases. For cost functions that exhibit BPs, exponentially many measurements may be required to determine the minimization direction in gradient-based optimization. This challenge in scaling applies not only to gradient-based optimization but also to derivative-free optimization methods, as discussed in Arrasmith et al. (18), and remains unresolved even with the application of higher-order optimization techniques (19). Research efforts have linked the BP problem to the overall expressiveness of the variational quantum circuit ansatz (20). Also, the degree of entanglement of the wave-function (21–24), and the non-locality of the cost function (17, 25, 26) have also high influence on encountering BPs during the optimization process. These findings imply that BPs are a fundamental property of variational quantum algorithms at scale, needing extra measures to mitigate their impact.

Numerous methods have been proposed to address this issue, but it remains uncertain whether these approaches can resolve the BP problem. Early research initiatives focused on strategies to circumvent BPs during the initialization phase of algorithms. For instance, Grant et al. (27)

suggested initializing the circuit with blocks containing identity gates. Skolik et al. (28) proposed optimizing the circuit layer by layer, while Dborin et al. (29) recommended employing a matrix product state ansatz for the optimization to reduce entanglement. An alternative strategy was formulated in the study of (30) to take advantage of correlated or restricted single-qubit rotation parameters (or direction). An alternative approach utilizing the method of natural gradient (31, 32) was also investigated in the literature and has been found to be a promising strategy compared to conventional gradient-based optimizers. Though, the individual optimization steps turned to be quite expensive and it's tolerance against BPs was not addressed.

Taking a different approach, the relationship between the occurrence of BPs and the structure of the cost function has been explored in references (17) and (25). Additionally, the introduction of concepts like entanglement-induced BPs (21) and noise-induced BPs (33) have added new routes to the discussion. The relation between BPs and entanglement has lead to various proposals that suggest controlling entanglement to mitigate BPs (22, 34–36). Furthermore, the idea of weak BPs, as defined for a subset of qubits (37), has been employed to detect early indicators of BPs and prevent them from occurring. In addition, (37) has demonstrated that entanglement-induced BPs and BPs arising from local cost functions are essentially the same. Therefore, strategies to avoid entanglement-induced BPs are equivalent to strategies for avoiding BPs associated with local cost functions. It's important to highlight that all of the suggested methods for mitigating BPs primarily focus on avoiding entering onto a BP in the first place. There is currently no known methodology to follow when the optimization process is already in the midst of a barren plateau. One might even argue that barren plateaus can be utilized to characterize the trainability of variational quantum algorithms: an algorithm shows better trainability when experiencing less impact from barren plateaus.

In this study, we turn over this reasoning and investigate the possibility to engineer a BP resistant optimization technique, showing lower degree of dependence on BP indicators like the

vanishing gradient components or high entanglement entropy. We present a novel evolutionary strategy that has proven to be remarkably effective in optimization, even when initiated from a point in the parameter space associated with high entanglement entropy. This optimization approach seamlessly integrates into the standard VQE framework, as it only requires the evaluation of the target cost function to be optimized. The idea to use evolutionary machine learning practices has been proven in several scenarios, trying to increase the training capabilities of variational quantum algorithms in the context of quantum architecture search (19, 38–43) Though, none of these studies delivered a viable approach to mitigate the consequences of BPs on the optimization process. Our novel evolutionary approach implemented in the SQUANDER circuit optimization package (44) attempts to fill this gap. We demonstrate the efficiency of our approach through various applications, including optimizing the ground state of the model like the XXX Heisenberg or the SYC model (45–47), and quantum gate compilation of deep circuits. Among the key advantages of our algorithm, we can also mention the computations cost of a single iteration do not exceed the complexity of a conventional gradient based approach optimizing over the same number of parameters. By evaluating distant features of the cost-function landscape, the optimization strategy can avoid flat areas and not even miss narrow valleys leading to acceptable solutions. While our studies are focusing on VQEs, they readily extend to other variational hybrid algorithms as well, such as quantum machine learning, quantum optimization or variational time evolution. The developed optimization algorithm can be also ported to realistic experiments performed on quantum processors, since it relies on the evaluation of the cost function with simple phase shifts applied on the parameters. We performed our numerical experiments using quantum computer simulations implemented in the SQUANDER package (44).

The structure of the paper is organized as follows. In the first section following the introduction we overview the concept of the VQE algorithm. Subsequently, we present the technical

background of our novel optimization method exploiting long-range properties of the optimization landscape to determine the search direction and performing evolutionary selection strategy to further increase the success rate to find the global minimum. In the third section we outline the concept of the entanglement entropy – BP link, using the second-Renyi entropy for BP inference. In the fourth section we present our numerical results on training quantum to approximate the ground states of the Heisenberg and SYC models. Finally, we conclude our work in the last section.

Brief description of the VQE algorithm

As implied by its name, VQE aims to approximate the ground state of a quantum system that is challenging to simulate using classical hardware. Thus, the first step in the VQE is to define the system for which we want to find the ground state. By providing a Hamiltonian \hat{H} and a trial wave-function $|\Psi\rangle$, the ground state energy associated with this Hamiltonian, E_0 , bounded by

$$E_0 \leq \frac{\langle \Psi | \hat{H} | \Psi \rangle}{\langle \Psi | \Psi \rangle} \quad (1)$$

The primary objective of VQE is to determine a parameterization for $|\Psi\rangle$ that minimizes the expectation value of \hat{H} . This expectation value serves as an upper bound for the ground state energy (48) and, in an ideal scenario, should be practically identical to it, meeting the desired level of precision. Therefore, VQE operates by variational optimization of the parameters within the quantum circuit ansatz.

To transform the minimization task into a quantum computer-executable problem, the first step is to define an ansatz quantum circuit used to prepare the trial wave-function on a quantum processor. Therefore, we represent $|\Psi\rangle$ as the result of applying a generic parameterized unitary operation $U(\theta)$ to an initial state of N qubits, with the parameter set denoted as θ , taking values in the range $(0, 2\pi]$. For simplicity, the qubit register is typically initialized as $|0\rangle^{\otimes N}$, denoted

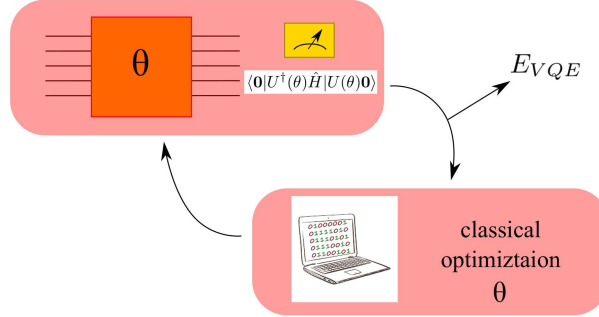


Figure 1: Schematic process of the VQE algorithm. The expectation value of the Hamiltonian is evaluated using the quantum processor parameterized with a parameter vector θ . The VQE energy is optimized via classical computer by updating the parameter vector θ provided for the quantum circuit in each iteration.

as $|0\rangle$. The VQE procedure is illustrated in Fig. 1. Given that $|\Psi\rangle$ must be a normalized wavefunction due to the unitary evolution, we can now formulate the VQE optimization problem as follows, omitting the normalization factor from Eq. (1):

$$E_{VQE} = \min_{\theta} \langle 0 | U^\dagger(\theta) \hat{H} | U(\theta) 0 \rangle \quad (2)$$

Equation (2) is referred to as the cost function in the context of the VQE optimization problem. This terminology is adopted from the fields of machine learning and mathematical optimization literature.

To implement the VQE algorithm on real quantum processors, a typical approach is to expand the Hamiltonian in terms of quantities that can be directly measured on a quantum device. This representation is often achieved by expressing the Hamiltonian as a weighted sum of Pauli spin operators. Observables suited for immediate measurement on a quantum device can be formed by tensor products of spin operators. These observables can be defined as Pauli strings denoted as $\hat{P}_\alpha \in I, X, Y, Z^{\otimes N}$, where N represents the number of qubits utilized in the quantum register. The Hamiltonian can then be reformulated as follows:

$$\hat{H} = \sum_{\alpha}^{\mathcal{P}} w_{\alpha} \hat{P}_{\alpha} \quad (3)$$

with w_α being a set of weights, and \mathcal{P} the number of Pauli strings in the Hamiltonian. Equation (2) then becomes

$$E_{VQE} = \min_{\theta} \sum_{\alpha}^{\mathcal{P}} w_\alpha \langle \mathbf{0} | U^\dagger(\theta) \hat{P}_\alpha | U(\theta) \mathbf{0} \rangle \quad (4)$$

where the terms $E_{P_a} = \langle \mathbf{0} | U^\dagger(\theta) \hat{P}_\alpha | U(\theta) \mathbf{0} \rangle$ corresponds to the expectation value of a Pauli string \hat{P}_α and can be measured by a quantum device, while the summation of these terms are calculated using a classical machine. Generally, to evaluate E_{VQE} with the aid of a quantum chip it is required to sample the expectation values of the Pauli strings several times. Typically, in order to attain a precision of ϵ for the expectation value of an operator, it is necessary to conduct approximately $\mathcal{O}(1/\epsilon^2)$ iterations of the circuit execution, each terminated by a measurement at the end [38]. Therefore, to increase the efficiency of the VQE execution measurement strategies are studied to minimize the number of the required repetitions [82,120,121].

Once the parameters θ have been successfully optimized, the trial state $|\Psi\rangle$ serves as a model for the system's ground state wave-function under investigation. Throughout the optimization process, the ansatz parameters must undergo iterative updates until convergence is achieved. Therefore, the selection of a classical optimization algorithm plays a crucial role. Firstly, it directly influences the number of measurements needed for each optimization step and the total number of iterations required to reach convergence. Secondly, specific optimization strategies have the potential to partially mitigate particular optimization challenges, such as the BPs problem [131–135]. Though, a full-fledged solution to handle BPs during the optimization process still forms an open challenge for researchers, as the proposed strategies rather aim to avoid BPs and not overcome them.

Evolutionary optimization technique to train quantum circuits

Evolutionary algorithms (49, 50) apply the principles of evolution found in nature to find the most optimal configuration of properties to accomplish specific tasks. They are often applied in scenarios where solving problem in polynomial time is not feasible, like in the case of combinatorial optimization problems, leading to NP-hard tasks at scale. In this sense, evolutionary algorithms optimize among different possibilities in the space of solution candidates, which are encoded in specific properties of the individuals, referred to as *agents* in the followings. Evolution is therefore based on recombination over a group of agents, accompanied with random mutations. Natural selection between the agents is performed according to the optimization criteria, encoded in the cost function. This process is repeated until the individuals can not improve any more in solving the optimization problem.

The agents explore the parameter space to find a favorable route that eventually decreases the cost function the most. A possible and numerically efficient scenario might be to follow a trajectory traced by the optimization of the cost function with respect to a small subset of the free parameters. In other words, the agents perform in each iteration an exact line search along the direction determined in a randomly selected parameter-subspace while keeping the rest of the parameters constant. Studies of Refs. (51) and (52) showed that by meeting certain conditions in the parameterization of the quantum gates, the single parameter dependence of the energy landscape in a VQA algorithm can be described by a simple sinusoidal function with a period of 2π . This finding has inspired the creation of two high performance optimization algorithm demonstrated in this work. First of all we should mention that merely three calls to the cost function are sufficient to find the exact minimum with respect to a single parameter. Secondly, global-scaled properties on the optimization landscape can be collected by sampling the cost function along single-parameter directions, leading to the formulation of a novel strat-

egy on deciding the search direction during the optimization iterations. These mathematical findings enable a monotone step-by-step reduction of the cost function by iteratively selecting a new subset of parameters during the optimization process. The result of the procedure is determined by both the starting point in the parameter space and the sequence of the chosen parameters. Unfortunately, neither the optimal starting point nor the most optimal parameter subset sequence is known in advance. While a predefined sequence of parameters, such as an iterative parameter sweep following a periodic pattern, might prematurely lead to convergence in most cases, a well-chosen sequence of optimized parameters could significantly enhance the overall optimization efficiency. In this work we show via numerical experiments, that probability based approaches promise a high success rate in finding a sub-optimal sequence of the optimized parameters.

Evolutionary selections The algorithm described in this study is based on a highly-efficient parameter-wise optimization routine and on an evolutionary selection of the sequence of the parameters over which the cost function is minimized. In our algorithm, each agent randomly selects the next parameters to be optimized by sampling from a uniform distribution. After optimizing the cost function with respect to the chosen parameters, agents pick up a next subset to optimize, again via uniform distribution sampling.

This repetitive process charts a path in the parameter space, over which the cost function is being optimized. Upon completing a specified number of iterations (set to a value between 200 and 20000 in our reference implementation within the SQUANDER package), the evolution of the agents are compared to each other and the most successful agent (returning the most favorable cost function) is selected. We refer to this step in the algorithm as *agent synchronization protocol*.

At this stage, the individual agents are randomly assigned to either continue their optimiza-

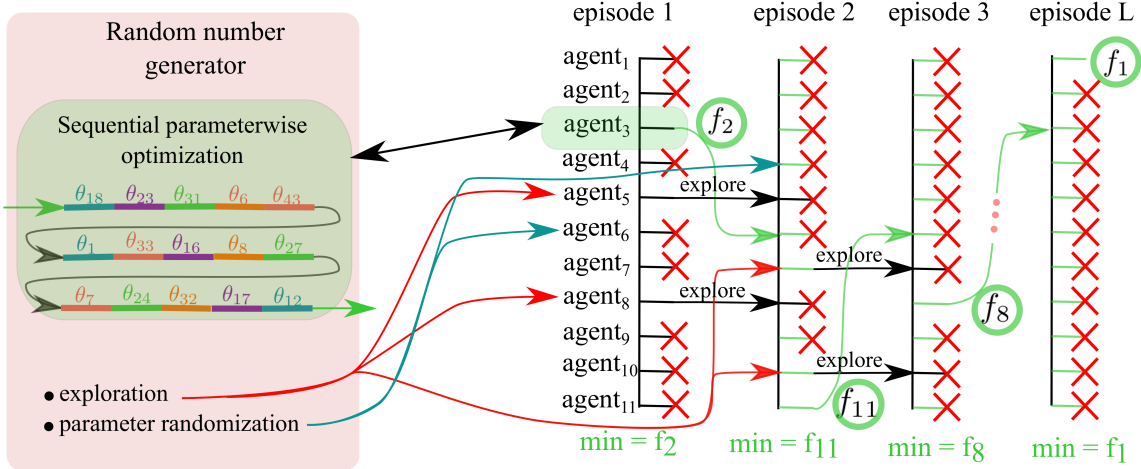


Figure 2: Illustration of the evolutionary algorithm in a corner case of a single-parameter optimization per iteration per step. In each episode the agents perform parameter-wise optimization along a path defined by a randomly chosen sequence of parameters. At the end of an epoch the most successful agent is selected and its state is spawned over the remaining agents for the next episode. The remaining agents are either terminated (indicated with red crosses), or randomly selected to keep their state and resume their evolution to further explore the parameter space (see the red arrows indicating the chosen agents). Some randomly chosen to implement a randomization on their state (see the blue arrows indicating the chosen agents). The figure illustrate a specific example with 11 agents, resulting in a sequence of best solutions $f_2 > f_{11} > f_8 > \dots > f_1$, with the final result f_1 after L episodes.

tion path with a probability of $p_{exploration}$ or start a new route from the actual position of the most successful agent. The latter option has a probability of $1 - p_{exploration}$. In the reference implementation of the algorithm $p_{exploration} = 0.2$ was chosen as default.

We split the optimization algorithm into episodes: each episode terminates with the described agent synchronization protocol and encompasses the evolution of the agents between two synchronization points. To further enhance the success rate through avoiding local minima of the energy landscape, the parameter vector associated with a given agent undergoes a perturbation with a probability $p_{randomization}$ right after the agent-synchronization protocol. This action causes an adjustment in the elements of the parameter vector by a randomly selected value from the range $[-r, r]$. In our reference implementation of the algorithm $p_{randomization} = 0.2$,

and $r = 0.3$ was chosen as default. The described algorithm is schematically visualized in Fig. 2.

Single parameter optimization The algorithm's performance is highly influenced by the efficiency of the line search that is commonly enhanced by performing inexact line search (53). Instead of finding the exact minimum in the search directions, an inexact line search terminates after finding an acceptably good point providing sufficient decrease in the cost function. In our case, however, the sinusoidal structure of the landscape enables to design an efficient method to find the exact minimum with respect to the chosen parameter just in few evaluation of the cost function. Firstly, the circuit can be decomposed into a sequence of single-parameter unitaries, each having a form $U_i = \exp(\theta_i \hat{H}_i)$, where \hat{H}_i is a hermitian matrix generating a rotation. Scaling this matrix allows each unitary U_i to be adjusted to have a period of 2π . Secondly, if \hat{H}_i s are full-rank matrices, the unitaries U_i s can't facilitate controlled rotations. Consequently, parameter-free entangling gates are added to the circuit which do not affect the sinusoidal nature of the single-parameter dependence of the cost function which reads as

$$E_{VQE} = \kappa \cdot \sin(2p_i + \xi) + C . \quad (5)$$

The derivation of this equation is straightforward as the state generated by the circuit can be given in the form

$$|\Psi\rangle = \cos(p_i)|a\rangle + \sin(p_i)|b\rangle \quad (6)$$

with respect to the parameter p_i , where $|a\rangle$ and $|b\rangle$ are normalized quantum states. By evaluating the expectation value $\langle \Psi | \hat{H} | \Psi \rangle$ we end up with Eq. (5) by introducing suitable constants κ , ξ and C . In this work we generalize this equation to cases when parametric controlled rotation gates are also incorporated in the circuit, particularly significant in certain approaches of quantum gate compilations (54, 55). In this scenario the general form of the cost function combines two

frequencies:

$$E_{VQE} = \kappa \cdot \sin(2p_i + \xi) + \gamma \cdot \sin(p_i + \phi) + C . \quad (7)$$

The extra sinusoidal term in this expression can be explained by the additional constant term $|c\rangle$ in the quantum state originating from controlled unitary gate operations. Namely, the state generated by the circuit as a function of the parameter p_i can be written in the form

$$|\Psi\rangle = \cos(p_i)|a\rangle + \sin(p_i)|b\rangle + |c\rangle \quad (8)$$

By evaluating the expectation value of the Hamiltonian, Eq. (7) can be recovered. Unlike the original setup with 3 cost function calls, in this case 5 samples are needed to fully recover the cost function and to solve the minimization problem with respect to a single parameter. For more details see the Sec. S2 of the supplementary material. Computationally, the increased number of the required function evaluations might question the application of this generalized approach, however, the enhanced expressibility of the circuit with parametric controlled rotations might improve the trainability of the circuit, which has been already proven in quantum gate compilation experiments (54, 55). In VQE experiments controlled rotation gates can be considered as an abstraction, encompassing two parameter-free controlled two-qubit gates and two single-qubit rotations with correlated angles of rotation. As was shown in the study of Refs. (56) and (30), correlated parameters in the circuits might increase their trainability.

Optimization over gradient-free multi-parameter search direction To further generalize the optimization approach and potentially improve its efficiency, we extend the concept of the parameter-wise optimization to a finite subset of the parameters. While this extension adds complexity to the line search phase of the optimization, it has the potential to result in much faster convergence of the solution.

As mentioned in the preceding section, it requires 3 function calls to determine the exact minimum of the cost function along a single parameter while keeping the others fixed. However,

if the function value at the initial point θ is known from the previous optimization iteration, the cost of determining the minimum with respect to a single parameter reduces to 2 function calls. Let's assume that at the start of the iteration step, a subset $\Lambda \subset 1, \dots, L$ of the parameters was randomly selected (where L is the total number of parameters). For each parameter θ_i with $i \in \Lambda$, the parameter-wise minimum θ_i^* was determined using Eq. (5). Then we define the search direction \mathbf{d} in the parameter space with components

$$d_i = \begin{cases} \theta_i^* - \theta_i & \text{if } i \in \Lambda \\ 0 & \text{otherwise.} \end{cases} \quad (9)$$

The method for determining the gradient-free search direction is illustrated schematically in Fig. 3. In each iteration, the search direction \mathbf{d} is established with respect to the randomly selected subset of parameters. Subsequently, a line search is conducted over the points of $\theta + t \cdot \mathbf{d}$ with $0 \leq t \leq 1$ to identify the point with the lowest cost function, which serves as the starting point for the next iteration.

Following the best practices applied in conventional gradient-based optimization methods, we incorporate an (gradient-free) inexact line search into the algorithm by taking a predefined number of equidistant samples from the cost function and selecting the point for the next iteration with the lowest value.

We assert that the described procedure will converge to either a global or local minimum, and this is ensured by two key properties of the algorithm. (i) Firstly, the cost function consistently decreases with each iteration. (ii) Secondly, any local minimum in the landscape is an attracting fixed-point of the optimization process. Therefore, like other optimization strategies, the described algorithm might get trapped in a local minimum as well. An avenue for significant enhancement could involve executing the optimization with multiple agents and implementing evolutionary selection among them, as detailed in a previous section. However, our numerical experiments have indicated that even with a single agent, the described algorithm proves to

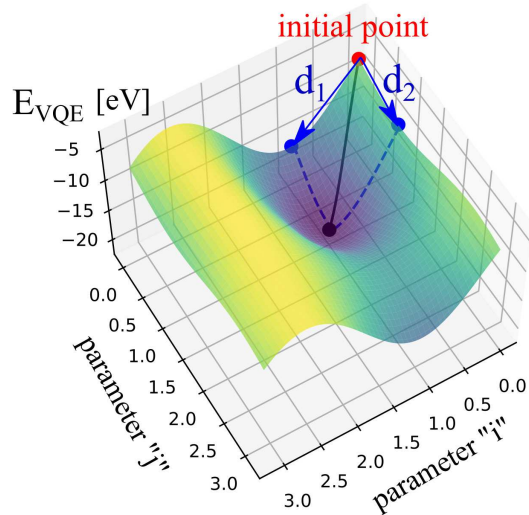


Figure 3: A typical E_{VQE} energy landscape as a function of two selected parameters " i " and " j ", while the other parameters are kept fixed. The blue colored arrows d_1 and d_2 label the two components of the search vector given by Eq. (9). The search vector determines the path of the line search between the initial (red colored) and minimal point (black colored). In the next iteration step a new line search is performed originating from the black point and optimizing over a new subset of parameters.

be quite efficient in training quantum circuits up to sizes accessible on classical simulators, as getting trapped in local minima showed to be highly unlikely.

Discerning BPs via monitoring the entropy of subsystems

As mentioned in the introduction, a high vale of entanglement (or von Neumann) entropy (57) is often accompanied with the occurrence of BPs in the optimization landscape. The rapid growing of the entanglement entropy server as an indicator of BP formation, making it a valuable monitoring tool during optimization. Inspired by these findings, we also use the concept of entropy monitoring during the optimization process to characterize the path in the parameter landscape passed during the optimization process.

Moreover, the study of ref. (37) introduces the concept of weak BPs (WBPs) as precursors of BPs. WBPs emerge when the entanglement of a local subsystem exceeds a certain threshold identified by the entanglement of a fully scrambled state. In contrast to BPs, WBPs can be efficiently diagnosed using the few-body density matrices via evaluating the second Rényi entropy, given by

$$S_2 = -\ln \text{Tr} \rho_A^2 . \quad (10)$$

Here $\rho_A = \text{tr}_B \rho$ is the reduced density matrix where A denotes the subset of qubits that are measured and B is the rest of the system. While in a simulation the evaluation of the entropy is straightforward, it's value can also be inferred experimentally. The algorithm introduced in (58), called classical shadow estimation, efficiently estimates the expectation value not only of the cost function and its gradients but also the second Rényi entropy of small-sized subsystems. For practical reasons, we will always normalize the second Rényi entropy by the Page entropy S_{Page} , which is the upper bound of the von Neumann entropy of a Haar random state (59):

$$S_{Page}(k, N) \approx k \ln 2 - \frac{1}{2^{N-2k+1}} . \quad (11)$$

Here k labels the number of qubits in the chosen subspace in the N -qubit register. Study of Ref. (37) showed that in the limit of (nearly) maximal possible entanglement of a small subregion A, the expected value of the second Rényi entropy comes close to the Page entropy.

Results

In this section, we present the outcomes of our numerical simulations conducted on variational problems, specifically the estimation of the ground state of an XXX Heisenberg Hamiltonian and the SYC model. In both of these models, the ground state satisfies volume law, indicating that the entanglement entropy of any bipartition of the state scales with the volume, i.e., $(\rho_A) \sim |A|$ (refer to Ref. (37) for a comprehensive review of these concepts). Additionally, we share numerical results obtained from quantum gate decomposition problem scenarios. Our findings demonstrate that the developed evolutionary algorithm excels in deep quantum circuit synthesis tasks, outperforming traditional optimization methods such as the well-known Broyden–Fletcher–Goldfarb–Shanno (BFGS) (60) or the ADAM (61) optimization methods. These traditional methods prove ineffective in producing meaningful results for the gate decomposition.

We conducted the training of the targeted quantum circuits utilizing the high-performance quantum computer simulator embedded in the SQUANDER package. To assess the capabilities of the new optimization technique, we deliberately excluded any noise in the simulation of the circuits and assumed perfect measurements on the qubits. This approach allowed us to concentrate specifically on the performance of the evolutionary optimizer across various applications and leave the impact of noise and other imperfections of a VQE experiment for future studies.

In the training of quantum circuits, we considered the circuit of the form of "hardware-

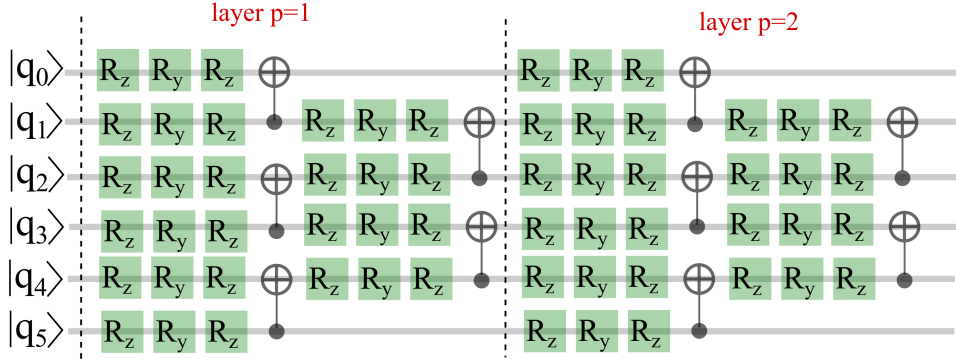


Figure 4: The structure of the "hardware-efficient" circuit ansatz used in our numerical experiments. The single qubit rotations are expressed by three consecutive rotations around axis Z , Y and Z again. The circuit ansatz is built from identical layers, denoted with the parameter p .

efficient" ansatz described by a unitary

$$U(\theta) = \prod_{i=1}^P \left(W_i \prod_{j=1}^N U_i^j(\theta_i^j) \right) . \quad (12)$$

The N -qubit circuit is composed from periodic layers of parameter-free entangling layers W_i and parametric single-qubit rotation layers composed from independent single-qubit rotations U_i^j acting on qubit j in the layer i . The entangling layers are composed from controlled-not (CNOT) gates connecting nearest neighbor qubits, as shown in Fig.4 for the case of 5 qubits.

Our initial objective in these numerical experiments is to demonstrate the efficient utilization of the gradient-free multi-parameter search direction in circumventing BPs during circuit training. To achieve this, we focus on a specific scenario in which only a single agent operates on a randomly chosen subset of the parameters. In this form, the strategy closely resembles traditional gradient descend optimization algorithms. The key difference is the incorporated routine to determine the search direction. While conventional gradient-based optimizers choose the search direction based on local properties of the cost-function landscape, such as the gradient or curvature, our proposed alternative approach suggests that determining the search direction via long-range properties of the optimization landscape yields superior results.

Our second objective was to enhance the optimization strategy by introducing mechanisms to prevent or significantly reduce the likelihood of getting trapped in local minima within the optimization landscape. To achieve this, we employed a multi-agent approach and implemented evolutionary selection among them.

We showcase the effectiveness of the evolutionary approach on quantum circuit synthesis problems, particularly in scenarios where our previous findings indicated the presence of local minima leading to the termination of most gradient-based optimizer processes. The gate synthesis problem emerged as a promising candidate to investigate the impact of evolutionary selection on the optimization’s success rate while maintaining a low level of complexity in the cost-function evaluation. This aspect of our numerical experiments is crucial, as optimization with evolutionary selection involves a significant amount of redundant calculations that need to be discarded.

Heisenberg XXX Model The Heisenberg model, composed in terms of the \hat{X} , \hat{Y} and \hat{Z} Pauli spin operators, encompasses the most general form of Hamiltonian that can be simulated on a qubit-based quantum processor. When scaled up, the Heisenberg model with randomly chosen coupled qubit pairs, becomes hard to simulate by classical means. The reason for this is attributed to the non-local interactions between the sites resulting in a volume-law entanglement scaling for a typical bipartite cut. Specifically, here we focus our study on k -local Hamiltonians \hat{H} , defined as sum of terms each containing at most k Pauli matrices. In our numerical simulations we take k to be finite and fixed, while the number of qubits $N \gg k$. A typical example describing such a model for $k = 2$ and including a bias term related to the effect of an external magnetic field is given by equation

$$\hat{H}_{XXX} = \sum_{i,j \in V_{\mathcal{G}}} J (\hat{\sigma}_i^z \hat{\sigma}_j^z + \hat{\sigma}_i^y \hat{\sigma}_j^y + \hat{\sigma}_i^x \hat{\sigma}_j^x) + h_z \sum_N \hat{\sigma}_i^z . \quad (13)$$

Despite of the local k -terms in the formula, according to the reasoning of Refs. (16, 17) the VQE formulation of such models will still exhibit BPs in a limit of $\mathcal{O}(\text{poly}(N))$ deep quantum circuits. Therefore, with a deep enough quantum circuit the VQE algorithm will also suffer from a BP, making this model to be a suitable test case to show the efficiency of the developed evolutionary optimization technique in training the circuit.

Sachdev–Ye–Kitaev model From theoretical point of view, the Sachdev–Ye–Kitaev (SYK) model- (45–47), with it’s non-local Hamiltonian structure in the Puali basis, is a frequently visited representative of variational problems that are proven to be hard to solve in VQE context. This is because the SYC model features a ground state that is nearly maximally entangled (47, 62), so crossing a BP becomes inevitable during the VQE process (34). From solid state physics point of view, the SYK model can be used to describe $2N$ spinless Majorana fermions χ_i satisfying the following anticommutation relations $\{\chi_i, \chi_j\} = \delta_{i,j}$. The Hamiltonian of the model reads as

$$\hat{H}_{SYC} = \sum_{1 \leq i < j < k < l \leq 2N} J_{i,j,k,l} \chi_i \chi_j \chi_k \chi_l , \quad (14)$$

where the couplings $J_{i,j,k,l}$ are taken randomly from a Gaussian distribution with zero mean and a variance of

$$\text{var}(J_{i,j,k,l}) = \frac{3!}{(N-3)(N-2)(N-1)} J^2 . \quad (15)$$

This fermionic Hamiltonian can be adopted to a quantum hardware by mapping the couplings between the Majorana fermions onto spin-chain variables by the nonlocal Jordan-Wigner transformation:

$$\chi_{2i} = \sigma_1^x \sigma_2^x \dots \sigma_{i-1}^x \sigma_i^y \quad \chi_{2i-1} = \sigma_1^x \sigma_2^x \dots \sigma_{i-1}^x \sigma_i^z . \quad (16)$$

such that $\{\chi_i, \chi_j\} = \delta_{i,j}$ will hold on. This encoding enables one to model $2N$ Majorana fermions with only N logical qubits. Generally speaking, we can consider the SYC model as a corner case of the Heisenberg model, when no restriction is made on the number of coupled

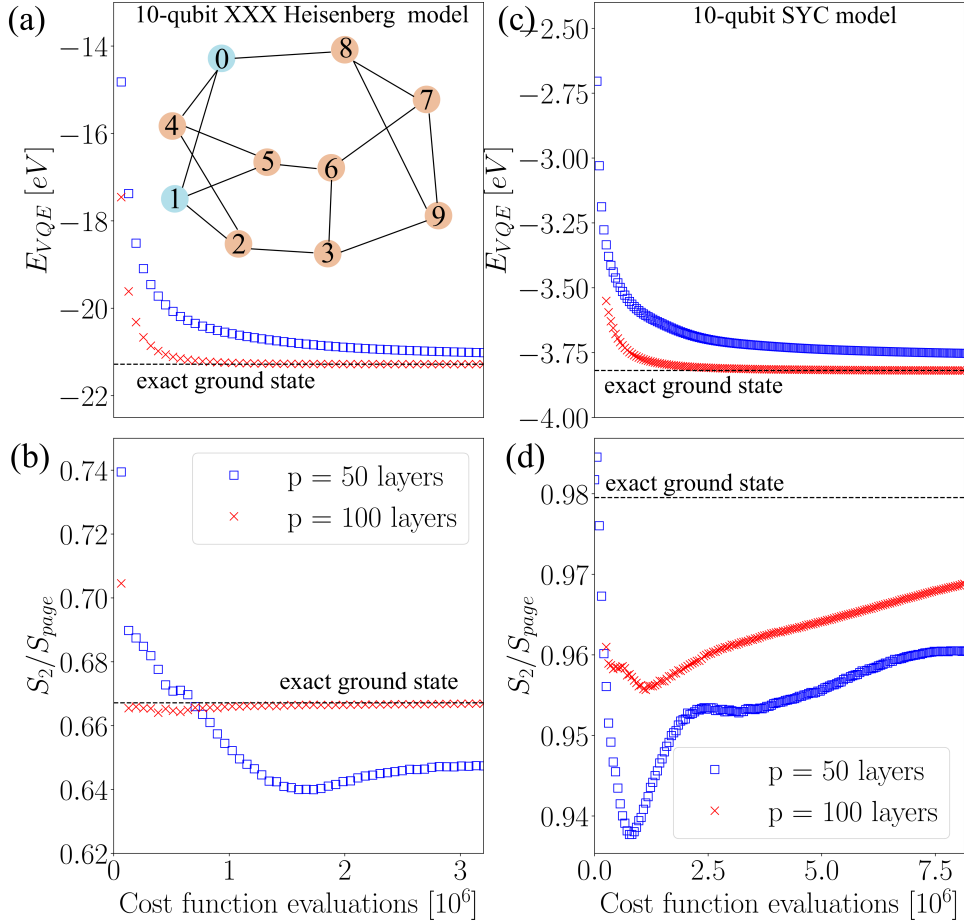


Figure 5: VQE simulations implementing the strategy based on the gradient-free multi-parameter search direction with a single agent. The training of the quantum circuits was conducted to find the ground state for the $N = 10$ -qubit XXX Heisenberg model on a 3-regular random graph depicted in the subset of sub-figure (a) and for a 10-qubit SYC model. Panels (a) and (b) show the evolution of the VQE energy and the normalized second-Rényi entropy evaluated on the sites 0 and 1 (labeled by blue in the insets) for the Heisenberg model. Sub-figures (c) and (d) show the same kind of results for the SYC model. The energy and the normalized entropy of the exact ground state for the Heisenberg system are $E_0 = -21.28$ eV and $S_2/S_{Page} = 0.667$. The exact ground state of the SYC model is $E_0 = -3.82$ eV with normalized entropy $S_2/S_{Page} = 0.980$. For the initialization we used random parameters.

qubits in a single term in the Hamiltonian. For our studies, we set $J = 1$ and consider a system of $N = 10$ qubits.

Numerical results In Fig. 5, we present the results of our numerical simulations conducted on 10-qubit Heisenberg XXX and SYC models. These systems have been recognized as challenging for VQE in numerous studies, and our tests with conventional gradient-based optimizers affirmed these observations. To address the optimization problem (2), we explored four strategies available within the SQUANDER package. The Powell-variant of the BFGS optimizer (63) and the Gradient Descent methods incorporate an inexact line search (53) in each iteration, proving to be quite efficient for smaller problems (e.g., in the synthesis of 3 – 5 qubit circuits). The handcrafted implementations of these optimizers also consider the periodicity of the optimization landscape by appropriately bounding the line search during optimization. Additionally, we included the ADAM optimization algorithm in our tests, although we did not implement the adaptive learning rate strategy proposed in (37). Our findings indicate that, despite exhaustive optimization and adaptation to quantum circuit training circumstances, these optimization engines struggle to solve these optimization problems at scale.

In contrary, our developed optimization algorithm demonstrated the ability to mitigate the effects of BPs in situations where other optimization methods fail. Notably, our approach avoids BPs without the need for external interventions or monitoring of specific quantities. As anticipated, in our numerical simulations, gradient-based optimization approaches became trapped near the energy level of the initial point.

The left side of Fig.5 illustrates our VQE experiments on a 10-qubit Heisenberg model identical to the system studied in (37). In each iteration step, we performed optimization by randomly selecting 64 parameters of the circuit and conducted a line search along the direction determined by Eq.(9). Throughout the iterations, we utilized a single agent, and no evolutionary

steps were applied during the simulations. Still, the optimization problem could be solved, while significantly reducing the computational complexity.

The outcome of this optimization process displayed a steady decrease in the VQE energy during the iterations [see Fig.5.(a)], while the evolution of the second-Renyi entropy demonstrated a rather non-trivial pattern [see Fig.5.(b)]. As the VQE instances in our simulations were initiated to random parameters, the entropy at the beginning of the optimization picked up large values implying large entanglement in the resulting state vector. However, as the optimization progressed, the entropy rapidly decreased, even falling below the value calculated from the exact ground state. Given that a sharp decrease in the evolution of the cost function generally correlates with low values of the second-Renyi entropy, this observation is expected. As the search direction and the bounds of the line search are determined via globally-scaled properties of the optimization landscape, the optimization process can navigate away from flat areas and avoid overstepping narrow valleys, guiding toward acceptable solutions.

Upon further analysis of the numerical results, it is valuable to explore the resulting properties of the quantum state $|\Psi(\theta)\rangle$ obtained via circuits of varying depths. In addition to examining the energy and entropy associated with the resulting state, a direct comparison between the state $|\Psi(\theta)\rangle$ and the exact ground state can be characterized by their overlap integral

$$M = |\langle \Psi_0 | \Psi(\theta) \rangle|^2 \quad (17)$$

Values of M close to 1 signify that the VQE wave function faithfully reproduces the exact ground state. On the left side of Fig.5, we compare a VQE optimization performed with circuits of depths $p = 50$ and 100 layers (refer to Fig.4 for the circuit structure). As depicted, with 100 layers, both the VQE energy and the second-Renyi entropy closely approach the theoretical results of the exact ground state. The overlap integral M calculated for the produced VQE state is also very close to 1, indicating that the VQE experiment successfully reproduced the exact

ground state with high accuracy. (The resulting VQE circuit with parameters can be accessed within the SQUANDER package (44)).

For a circuit with 50 layers, on the other hand, we could not approximate the ground state with such high quality. Neither the energy nor the entropy [plotted in blue in Fig. 5.(a)-(c)] fully converged to the values corresponding to the exact ground state. The overlap integral at the end of the optimization (terminated at $\sim 3 \times 10^6$ cost function calls) is $M = 0.97$. The results obtained for even shallower circuits rapidly become inaccurate. The explanation behind this observation is related to the expressiveness of the circuits. Considering 10 qubits, a general wave-function can be described by $2^{10} = 1024$ complex amplitudes, resulting in $2 \times 2^{10} - 2 = 2046$ free parameters (two parameters are constrained since the state is normalized). The 50-layered VQE circuit has 2700 free parameters, while the 100-layered variant can be tuned with 5400 free parameters. As one can see, the 50-layered circuits contain enough parameters to encode any quantum state, but the convergence slows down at the end of the optimization. The 100-layered circuit converges much faster to the solution, as it is likely over-parameterized.

Our results obtained for the SYC model further validate these considerations. As depicted in the right panels of Fig. 5, the VQE optimization for the SYC model exhibits similar behavior to the Heisenberg model on the left. With $p = 100$ layers in the circuit ansatz, we achieved a decent approximation of the ground state energy. In contrast, at $p = 50$ layers, the approximation becomes less accurate after 6.5×10^{-6} evaluations of the cost function. The second-Renyi entropy remains high throughout the optimization process, though it does not hinder the optimizer from obtaining high-quality results.

Regarding the exact solution of the SYC model, we need to mention that the diagonalization of the SYC Hamiltonian revealed a 2-fold degeneracy of the states. In addition, the 2-fold ground state and the nearest excited states (also 2-fold degenerate) were close to each other in energy. While the energy of the ground state was $E_{0,SYC} = -3.819$ eV, the first excited

energy was $E_{1,SYC} = -3.799$ eV. The VQE energy obtained with the training of the $p = 100$ layered circuit turned out to be $E_{VQE} = 3.814$ eV, a value that falls between the ground state energy and the first excited energy. Thus, the VQE state is expected to have a finite component orthogonal to the subspace of the 2-fold ground state. Fortunately, this orthogonal component has only an overlap $M = 0.098$ with the subspace of the first excited states, while the overlap of the VQE wave function with the subspace of the 2-fold ground state is $M = 0.902$. Hence, the components of the VQE wave function predominantly come from the ground state and the first excited state.

At this point we would like to also mention that the optimization Ref. (37) was not able to solve neither the same Heisenberg model nor the SYC model of identical size with an accuracy comparable to our results. (We also notice that (37) used slightly different circuit ansatz compared to ours.)

After examining 10-qubit systems, we raise the stakes and turn our attention to even more challenging problems. While it is not a significant challenge for quantum computer simulators to execute circuits beyond 20 qubits, the VQE experiments become quite expensive at this scale due to the large number of cost function evaluations. Therefore, in this work, we limit our considerations to problems up to 16 qubits. The goal of our VQE experiments is to reproduce the ground state of a randomly generated 16-qubit XXX Heisenberg model (with $k = 3$), as visualized in the inset of Fig. 6.(c). Furthermore, to increase the efficiency of the optimization process, we initiate the training of the circuits with parameter values equal to 0. Since the circuits are applied to the initial state $|0\rangle$ and initially, all the single-qubit rotations will be identities with this choice, the two-qubit entangling gates will lose their effect as well. This is because all the control qubits are initially in state 0, so the controlled two-qubit gates incorporated into the circuit will act as an identity gate as well. Consequently, the resulting state will have zero initial entanglement entropy, promising a steep initial descent in the VQE energy. De-

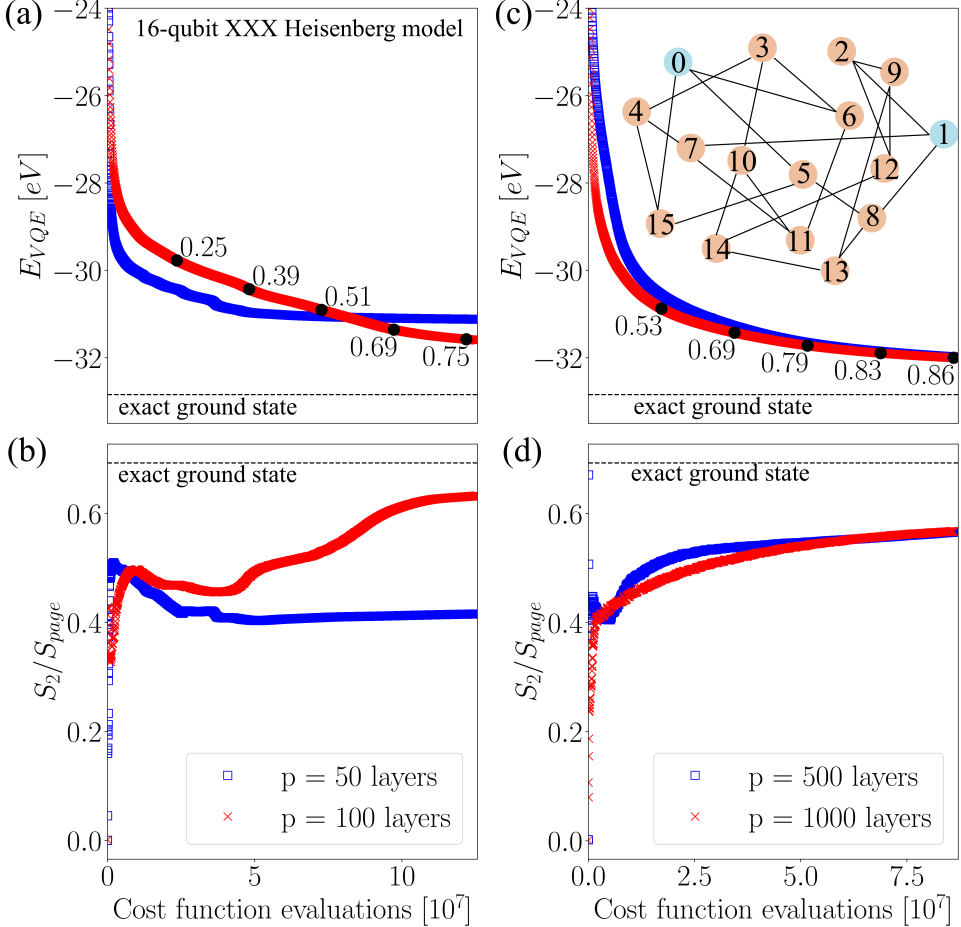


Figure 6: VQE simulations implementing the strategy based on the gradient-free multi-parameter search direction with a single agent. The training of the quantum circuits was conducted to find the ground state for the $N = 16$ -qubit XXX Heisenberg model on a 3-regular random graph depicted in the subset of subfigure (c). Panels (a) and (b) show the evolution of the VQE energy and the normalized second-Rényi entropy on sites 0 and 1 (labeled by blue in the insets) for the Heisenberg model evaluated with shallower circuits consisting of $p = 50$ and 100 layers, while . Subfigures (c) and (d) show the same kind of results obtained with deep circuits consisting of $p = 500$ and 1000 layers. The black numbers and dots represent the evolution of the of the overlap integral between the VQE wave function and the exact ground state defined by Eq.(17). The energy and the normalized entropy of the exact ground state for the Heisenberg system are $E_0 = -32.84$ eV and $S_2/S_{Page} = 0.693$. The optimization was initialized with parameters equal to 0.

spite of this simplification, our method remains autonomous in avoiding BPs on its own, there is still no need for any external intervention during the optimization.

A general 16-qubit wave function can be characterized by $2^{16} - 2 = 131070$ parameters. Consequently, circuits with either $p = 50$ or $p = 100$ layers are expected to provide much less accurate VQE wave functions than in the previously addressed 10-qubit case, where the number of trainable parameters in the circuit was sufficiently large. In the 16-qubit case, the 100-layered circuit ansatz contains only 9000 free parameters, which is much less than required to approximate the target state. The left panels of Fig.6 show the numerical results of the conducted VQE experiments with circuits consisting of $p = 50$ and $p = 100$ layers. As expected, it was not possible to precisely approximate the ground state energy in these instances (VQE energy of -31.1 eV with the 50-layered circuit and -31.6 eV with the 100-layered circuit). The 100-layered circuit gave significantly better results than those achieved with the 50-layered circuit. However, neither of these circuits could get close to the exact ground state energy of the model. After more than 10^8 evaluations of the cost function, the VQE wave function still showed a significant difference compared to the exact ground state, and the overlap calculated with the wave function generated by the 100-layered circuit did not exceed the value of $M = 0.75$. The black numbers in Fig.6.(a) indicate the evolution of the overlap with the number of cost function evaluations. As mentioned, these findings were not surprising, as the number of trainable parameters in these circuits was only 4500 and 9000 for the 50- and 100-layered circuits, respectively. The expressiveness of these circuits lags behind the numbers needed for the accurate approximation of a general 16-qubit wave function. Therefore, we increased the number of layers in our circuit ansatz by an order.

The right panels of Fig.6 show our numerical results obtained with these deep circuits composed of $p = 500$ and $p = 1000$ layers. As the plotted results indicate, the developed optimization strategy had no difficulties proceeding with the training of these deep circuits. We

still executed only a single agent in these numerical experiments, and optimized 128 parameters in each iteration. We observed that the efficiency of the optimization varies from run to run. Fig.6 shows the most successful executions, while in several experiments, we observed signs of convergence to a local minimum around the energy level of ~ -29 eV. We argue that this issue could be resolved by increasing the number of agents in the process due to the evolutionary selection of the most successful agents. However, due to the overwhelming numerical requirements of the performed VQE simulations, we did not try out this approach in these simulations. We revisit this aspect of the algorithm in the next section by addressing quantum gate synthesis problems, where it becomes essential to avoid local minima to retrieve meaningful results. In these experiments, evolutionary selection will play a crucial role in solving the addressed problems.

In the conducted 16-qubit VQE optimization our numerical simulation yielded a VQE energy of $E_{VQE} = -31.99$ eV with $p = 500$ layers and $E_{VQE} = -32.00$ eV with $p = 1000$ layers after 8×10^7 cost function evaluation, at which point the converge towards the exact ground state energy has dramatically slowed down. The largest value of the overlap integral (17) with the exact ground state turned to be $M = 0.86$.

Our numerical results highlight two main conclusions: (i) Firstly, the probabilistic algorithm developed in this work, making use of the global properties of the optimization landscape, is a promising candidate capable of solving variational quantum problems at scale, even beyond the capabilities of classical quantum computer simulators. (ii) Secondly, when using a general circuit ansatz to perform VQE optimization (like the circuit structure used in our experiments), highly accurate results require an exponentially scaling number of layers in the circuit ansatz. We acknowledge that the circuit ansatz used in our calculations may not be the most efficient one to model the ground states of the studied models. Ansatz structures accounting for the symmetry of the addressed physical model might significantly reduce the circuit depth for practical

applications (64–66). Our aim in this work was to examine the numerical capabilities of the new solver strategy. The non-efficient representation of the circuit ansatz did not impose limitations on us in achieving this goal. On the contrary, we could execute quite deep circuits and demonstrate that our strategy can be successfully applied even under extreme circumstances.

Quantum compilation of deep circuits A commonly employed approach in the compilation and optimization of large quantum circuits involves partitioning the circuit into smaller blocks that can be individually optimized or re-synthesized. This allows for the treatment of wide quantum circuits, as demonstrated in the work of Ref. (67), where circuits ranging from 4 to 400 qubits were addressed. Previous approaches following this partitioning strategy (68) were shown to scale to similar circuit sizes but were practically limited to using only 3-qubit sized partitions due to inefficient numerical optimization. In the experiments of Ref. (67), this limitation was overcome, extending the partition size to 6 qubits. The choice of the number of qubits per partition is crucial, as more qubits are likely to capture additional domain-level physical interactions, leading to improved optimization opportunities.

On the contrary, for partitions containing more qubits, the optimization problem becomes exceptionally challenging for traditional gradient-based solvers due to the dense presence of local minima in the landscape (54, 69). Here, we demonstrate that the evolutionary optimization algorithm described in this study enables the application of the adaptive gate synthesis approach of Ref. (54) to problems that were found to be intractable with conventional optimization engines, such as the BFGS method (54). In order to measure the distance between the initial unitary U of the quantum program and the synthesized unitary V (obtained from the synthesized circuit) we used the frobenius norm given by

$$f(U, V) = \frac{1}{2} \|V - U\|_F^2 = d - \text{Re} [\text{Tr}(U^\dagger V)], \quad (18)$$

with d being the dimension of the Hilbert-space. For further details of the decomposing al-

gorithm please refer to either Ref. (54) or to Ref. (69). Our numerical experiences revealed

Circuit name	qubits	Initial <i>CNOT</i>	QISKit <i>CNOT</i>	Ref (54, 69)		SQUANDER (44)	
				<i>CNOT</i>	\bar{T} [s]	<i>CNOT</i>	\bar{T} [s]
4gt5_76	5	46	529	24	1711	22	79
4gt10-v1_81	5	66	372	39	65737	37	2245
one-two-three-v1_99	5	59	302	45	80390	35	4693
one-two-three-v0_98	5	65	213	61	175994	42	20313
one-two-three-v2_100	5	32	502	37	5141	27	2687
4mod7-v1_96	5	72	150	33	10255	26	2951
aj_e11_165	5	69	337	36	15585	23	2823
alu-v2_32	5	72	469	41	33820	31	1639
alu-v4_36	5	51	193	40	11090	28	2106
4gt5_77	5	58	338	19	2855	17	483
4gt12-v0_86	6	116	1837	-	-	40	8174
4gt12-v0_87	6	112	1837	47	-	36	8598
4gt12-v0_88	6	86	1837	44	-	36	6577

Table 1: *CNOT* gate count comparison of deep 4 – 6-qubit circuits obtained by decomposing and optimizing unitaries taken from the online database (70). The individual columns label the name of the circuit, the number of qubits in the circuit, the initial *CNOT* gate count of the circuit, the *CNOT* gate count of the quantum circuit synthesized by QISKit transpile function. The last four columns show the *CNOT* count and average execution times obtained from Refs. (54) and (69), and the same kind of results obtained with the new evolutionary algorithm with the SQUANDER package. The final error f of the approximation calculated via Eq. (18) was less than 10^{-8} in each decomposition corresponding. We performed the benchmark calculations on a computing server equipped with 32-Core AMD EPYC 7542 Processor (providing 64 threads with multi-threading) and with 128GB of memory.

that quantum gate synthesis provides a perfect opportunity to explore problems where the presence of local minima in the optimization landscape causes traditional optimizers to fail, even at smaller scales. In our experiments, we observed that employing the developed evolutionary algorithm with multiple agents is indeed necessary to synthesize deep circuits while achieving a significant reduction in gate count. We executed 64 concurrent agents and synchronizing their evolution after 200 – 2000 optimization steps. To reduce the computational footprint, we limited the randomly chosen set of parameters to contain only a single parameter. Neverthe-

less, the developed evolutionary algorithm demonstrated exceptional efficiency in solving the addressed problems. For optimal performance, we combined the evolutionary algorithm with the BFGS strategy, switching to the latter when the cost function was reduced down to 10^{-3} by the evolutionary algorithm. The results of our numerical experiments are presented in Table. 1. Comparing these results with previous findings, we can draw two conclusions. Firstly, the average execution time was reduced by an order of magnitude in all addressed use cases where comparisons could be made. Secondly, the evolutionary algorithm exhibited remarkable stability and efficiency in solving the optimization problem with a precision of 10^{-8} .

Complexity considerations It is worth to study the computational complexity of the developed evolutionary algorithm described in this study. There are two key components in relation with our optimization technique characterizing it's cost. These are the utilization of the agents undergoing evolutionary selections and the size of the parameter subset over which the cost function gets optimized. Both of these dimensions, though, fall back to the count of sampling from the single parameter cross sections of the cost function. Since the terminating point of the line search can be reused in the next iteration, only 2 cost function evaluations are needed to reconstruct the parameter dependence of the cost function, if Eq. (5) is used to characterize the optimization landscape. In the more general case of Eq. (7) 4 cost function evaluations are required to determine the minimum with respect to a single parameter. Therefore, $2LM$ (or $4LM$) cost function evaluations are required to determine the search direction, and additional constant number of evaluations to perform the (inexact) line search. These numbers compare close to the case of regular gradient descend method. In particular, on a quantum computer the general rule of parameter shift (71) can be used to evaluate a gradient component of the cost function with 2 evaluations of the cost function. By carefully planning the number of agents and the number of optimized parameter components per iteration, the overall complexity of our

optimization algorithm can be set not to exceed the complexity of conventional gradient based methods.

Discussion

In this manuscript, we have presented a novel optimization method for training quantum circuits. A prevalent challenge in variational quantum algorithms is the hindering impact of barren plateaus (BPs) on circuit training. The vanishing gradient problem associated with BPs significantly limits the applicability of near-term quantum algorithms. Clearly speaking, the application of a given variational algorithm becomes questionable when the training process fails at large scaled problem instances. Therefore, developing optimization strategies resistant to BPs is highly desirable. We demonstrated that the long-range properties of the optimization landscape can be leveraged to determine a search direction and optimization bounds along this direction. This method introduces a novel line-search approach for training quantum circuits, autonomously maintaining low values of the second-Renyi entropy during optimization. Given the inherent connection between entropy and BPs, this property of the developed algorithm implies a natural tendency to avoid BPs during training without requiring external control mechanisms.

We applied the optimization strategy to VQE simulations on randomly generated Heisenberg XXX and Sachdev–Ye–Kitaev (SYC) models, all of which were previously identified to exhibit barren plateaus (BPs) during VQE process. We increased the depth of the training circuits to $p = 1000$ entangling layers with 16 qubits. The developed optimization strategy, utilizing the gradient-free search direction method, consistently decreased the VQE energy over thousands of iterations without getting trapped by BPs. We demonstrated these outstanding capabilities of the solver by training quantum circuits containing up to 15000 entangling gates.

In this study we also addressed another common issue of optimization approaches: the local

minima scattered over the optimization landscape causes early termination of the optimization and prevents from solving the addressed problem. This issue is particularly critical for quantum gate synthesis, where only results close to the global minimum are acceptable. Our numerical experiments demonstrated a significant increase in efficiency to avoid local minima and converge to the global minimum when employing evolutionary selection of agents. In most of the studied circuits, we achieved a substantial reduction in gate count and decreased the computational time by an order of magnitude. For these experiments, we utilized single-parameter optimization to keep computational requirements low.

We believe that the optimal training performance for large-scale variational quantum calculations can be achieved through the combination of these practices. However, due to the exponential scaling of quantum circuit simulation with the number of qubits, the limitations of classical computers have prevented us from conducting exhaustive research by applying the gradient-free multi-parameter search direction strategy and evolutionary selection in combination.

Combining the described probabilistic optimization strategy with machine learning practices has the potential to further improve its performance. Replacing the probability-based selection with machine learning inference could significantly reduce the number of redundant evaluations of the cost function during circuit training. We leave the exploration of this possibility for future research projects.

Acknowledgments

Founding: This research was supported by the Ministry of Culture and Innovation and the National Research, Development and Innovation Office within the Quantum Information National Laboratory of Hungary (Grant No. 2022-2.1.1-NL-2022-00004), by the ÚNKP-22-5 New National Excellence Program of the Ministry for Culture and Innovation from the source of the

National Research, Development and Innovation Fund, and by the Hungarian Scientific Research Fund (OTKA) Grants No. K134437 and FK135220. RP. acknowledge support from the Hungarian Academy of Sciences through the Bolyai János Stipendium (BO/00571/22/11) as well. We acknowledge the computational resources provided by the Wigner Scientific Computational Laboratory (WSCLAB) (the former Wigner GPU Laboratory).

Data and materials availability: The compiled quantum circuits reported in this work and the VQE trained circuits are publicly available within the SQUANDER package in QASM and other binary formats at GitHub repository (44)

References

1. A. Peruzzo, *et al.*, *Nature Communications* **5**, 4213 (2014).
2. J. R. McClean, J. Romero, R. Babbush, A. Aspuru-Guzik, *New Journal of Physics* **18**, 023023 (2016).
3. J. Tilly, *et al.*, *Physics Reports* **986**, 1 (2022). The Variational Quantum Eigensolver: a review of methods and best practices.
4. Y. Cao, J. Romero, A. Aspuru-Guzik, *IBM Journal of Research and Development* **62**, 6:1 (2018).
5. N. S. Blunt, *et al.*, *Journal of Chemical Theory and Computation* **18**, 7001 (2022).
6. V. Lordi, J. M. Nichol, *MRS Bulletin* **46**, 589 (2021).
7. A. Kandala, *et al.*, *Nature* **549**, 242 (2017).
8. G. A. Quantum, *et al.*, *Science* **369**, 1084 (2020).
9. Y. Cao, *et al.*, *Chemical Reviews* **119**, 10856 (2019).

10. M. P. Harrigan, *et al.*, *Nature Physics* **17**, 332 (2021).
11. N. Lacroix, *et al.*, *PRX Quantum* **1**, 020304 (2020).
12. V. Havlíček, *et al.*, *Nature* **567**, 209 (2019).
13. S. Johri, *et al.*, *npj Quantum Information* **7**, 122 (2021).
14. L. Bittel, M. Kliesch, *Phys. Rev. Lett.* **127**, 120502 (2021).
15. D. Wecker, M. B. Hastings, M. Troyer, *Phys. Rev. A* **92**, 042303 (2015).
16. J. R. McClean, S. Boixo, V. N. Smelyanskiy, R. Babbush, H. Neven, *Nature Communications* **9**, 4812 (2018).
17. M. Cerezo, A. Sone, T. Volkoff, L. Cincio, P. J. Coles, *Nature Communications* **12**, 1791 (2021).
18. A. Arrasmith, M. Cerezo, P. Czarnik, L. Cincio, P. J. Coles, *Quantum* **5**, 558 (2021).
19. M. Cerezo, P. J. Coles, *Quantum Science and Technology* **6**, 035006 (2021).
20. A. A. Holmes, H. J. Changlani, C. J. Umrigar, *Journal of Chemical Theory and Computation* **12**, 1561 (2016).
21. C. Ortiz Marrero, M. Kieferová, N. Wiebe, *PRX Quantum* **2**, 040316 (2021).
22. T. L. Patti, K. Najafi, X. Gao, S. F. Yelin, *Phys. Rev. Res.* **3**, 033090 (2021).
23. Z. Holmes, *et al.*, *Phys. Rev. Lett.* **126**, 190501 (2021).
24. K. Wang, Z. Song, X. Zhao, Z. Wang, X. Wang, *npj Quantum Information* **8**, 52 (2022).

25. A. V. Uvarov, J. D. Biamonte, *Journal of Physics A: Mathematical and Theoretical* **54**, 245301 (2021).
26. K. Sharma, M. Cerezo, L. Cincio, P. J. Coles, *Phys. Rev. Lett.* **128**, 180505 (2022).
27. E. Grant, L. Wossnig, M. Ostaszewski, M. Benedetti, *Quantum* **3**, 214 (2019).
28. A. Skolik, J. R. McClean, M. Mohseni, P. van der Smagt, M. Leib, *Quantum Machine Intelligence* **3**, 5 (2021).
29. J. Dborin, F. Barratt, V. Wimalaweera, L. Wright, A. G. Green, *Quantum Science and Technology* **7**, 035014 (2022).
30. Z. Holmes, K. Sharma, M. Cerezo, P. J. Coles, *PRX Quantum* **3**, 010313 (2022).
31. T. Haug, M. S. Kim, Optimal training of variational quantum algorithms without barren plateaus (2021).
32. D. Wierichs, C. Gogolin, M. Kastoryano, *Phys. Rev. Res.* **2**, 043246 (2020).
33. S. Wang, *et al.*, *Nature Communications* **12**, 6961 (2021).
34. J. Kim, Y. Oz, *Journal of Statistical Mechanics: Theory and Experiment* **2022**, 073101 (2022).
35. J. Kim, Y. Oz, *Phys. Rev. A* **106**, 052424 (2022).
36. R. Wiersema, C. Zhou, J. F. Carrasquilla, Y. B. Kim, *SciPost Phys.* **14**, 147 (2023).
37. S. H. Sack, R. A. Medina, A. A. Michailidis, R. Kueng, M. Serbyn, *PRX Quantum* **3**, 020365 (2022).
38. Y. Du, T. Huang, S. You, M.-H. Hsieh, D. Tao, *npj Quantum Information* **8**, 62 (2022).

39. S. Y.-C. Chen, *Proceedings of the 2023 International Workshop on Quantum Classical Cooperative*, QCCC '23 (Association for Computing Machinery, New York, NY, USA, 2023), p. 17–20.

40. U. Las Heras, U. Alvarez-Rodriguez, E. Solano, M. Sanz, *Phys. Rev. Lett.* **116**, 230504 (2016).

41. Z. Lu, P.-X. Shen, D.-L. Deng, *Phys. Rev. Appl.* **16**, 044039 (2021).

42. H. L. Tang, *et al.*, *PRX Quantum* **2**, 020310 (2021).

43. L. Ding, L. Spector, *Proceedings of the Genetic and Evolutionary Computation Conference Companion*, GECCO '22 (Association for Computing Machinery, New York, NY, USA, 2022), p. 2190–2195.

44. Sequential quantum gate decomposer, <https://github.com/rakytap/sequential-quantum-gate-decomposer> (2021).

45. A. Kitaev, A simple model of quantum holography (2015).

46. S. Sachdev, J. Ye, *Phys. Rev. Lett.* **70**, 3339 (1993).

47. J. Maldacena, D. Stanford, *Phys. Rev. D* **94**, 106002 (2016).

48. G. Arfken, H. Weber, *Mathematical Methods for Physicists* pp. 957–961 (1985).

49. D. Fogel, *IEEE Transactions on Neural Networks* **5**, 3 (1994).

50. T. H. W. Bäck, *et al.*, *Evolutionary Computation* **31**, 81 (2023).

51. K. M. Nakanishi, K. Fujii, S. Todo, *Phys. Rev. Res.* **2**, 043158 (2020).

52. M. Ostaszewski, E. Grant, M. Benedetti, *Quantum* **5**, 391 (2021).

53. *Line Search Methods* (Springer New York, New York, NY, 2006), pp. 30–65.
54. P. Rakyta, Z. Zimborás, Efficient quantum gate decomposition via adaptive circuit compression (2022).
55. N. A. Nemkov, E. O. Kiktenko, I. A. Luchnikov, A. K. Fedorov, *Quantum* **7**, 993 (2023).
56. T. Volkoff, P. J. Coles, *Quantum Science and Technology* **6**, 025008 (2021).
57. I. Bengtsson, K. Zyczkowski, *Geometry of Quantum States: An Introduction to Quantum Entanglement* (Cambridge University Press, 2006).
58. H.-Y. Huang, R. Kueng, J. Preskill, *Nature Physics* **16**, 1050 (2020).
59. S. K. Foong, S. Kanno, *Phys. Rev. Lett.* **72**, 1148 (1994).
60. C. Kelley, *Iterative Methods for Optimization*, Frontiers in Applied Mathematics (Society for Industrial and Applied Mathematics, 1999).
61. D. P. Kingma, J. Ba, Adam: A method for stochastic optimization (2014).
62. Y. Huang, Y. Gu, *Phys. Rev. D* **100**, 041901 (2019).
63. M. J. D. Powell, *Mathematical Programming* **38**, 29 (1987).
64. B. O’Gorman, W. J. Huggins, E. G. Rieffel, K. B. Whaley, Generalized swap networks for near-term quantum computing (2019).
65. G.-L. R. Anselmetti, D. Wierichs, C. Gogolin, R. M. Parrish, *New Journal of Physics* **23**, 113010 (2021).
66. J. S. Kottmann, *Quantum* **7**, 1073 (2023).

67. A. Kukliansky, E. Younis, L. Cincio, C. Iancu, Qfactor: A domain-specific optimizer for quantum circuit instantiation (2023).
68. X.-C. Wu, M. G. Davis, F. T. Chong, C. Iancu, *2021 International Conference on Rebooting Computing (ICRC)* (2021), pp. 35–46.
69. P. Rakyta, *et al.*, *Journal of Computational Physics* **500**, 112756 (2024).
70. A. P. A. Zulehner, R. Wille, https://github.com/iic-jku/ibm_qx_mapping (2019).
71. D. Wierichs, J. Izaac, C. Wang, C. Y.-Y. Lin, *Quantum* **6**, 677 (2022).